Geologica Acta, Vol.11, Nº 2, June 2013, 195-214
DOI: 10.1344/105.000001839
Available online at www.geologica-acta.com

geologica acta

Diagenetic processes in a partially dolomitized carbonate reservoir: Casablanca oil field, Mediterranean Sea, offshore Spain

N. RODRÍGUEZ-MORILLAS [1,2] **E. PLAYÀ** [1] **A. TRAVÉ** [1] **J.D. MARTÍN-MARTÍN** [1,3]

[1] **Departament de Geoquímica, Petrologia i Prospecció Geològica, Facultat de Geologia, Universitat de Barcelona**
C/ Martí i Franqués, s/n, 08028 Barcelona. (Spain). E. Playà E-mail: eplaya@ub.edu A. Travé E-mail: atrave@ub.edu, J.D. Martín-Martín E-mail: juandiegomartin@ub.edu

[2] **Centro Tecnológico de Repsol**
Ctra. Extremadura Km. 18, 28935, (Spain) Móstoles. N. Rodríguez-Morillas E-mail: noelia.rodriguez@repsol.com

[3] **Institute of Earth Sciences Jaume Almera ICTJA-CSIC, Group of Dynamics of the Lithosphere (GDL)**
C/ Lluís Solé i Sabarís s/n, 08028 Barcelona (Spain)

ABSTRACT

Mesozoic and Neogene carbonates located in the Valencia Trough (offshore Spain, western Mediterranean Sea) are oil reservoirs. This paper investigates the diagenetic evolution of the Upper Jurassic limestones, currently dolomitized, that constitute the main reservoir of the Casablanca oil field. Core samples from Casablanca-1A well have been studied to determine the diagenetic products and their relation with porosity evolution, and to reconstruct the fluid flow history prior to and during oil emplacement.

On the basis of petrological observations and geochemical analyses (major, minor and trace element composition and oxygen, carbon and strontium isotope composition), a major dolomitization event is recognized postdating subaerial exposure, erosion and karstification. The dolomitization event originated two replacive dolomites (RD1 and RD2) and two dolomite cements (saddle dolomite cement, SDC, and milky-white dolomite cement, MDC) which are partially cogenetic. RD1, RD2 and SDC precipitated at increasing temperatures (over 60ºC and below 110ºC), probably from meteoric water mixed with marine water. The last dolomite type (milky-white dolomite cement) precipitated with increasing burial conditions and by arrival of hydrothermal fluids during the Miocene. The post-dolomitization sequence comprises precipitation of calcite cement and partial calcitization of all previous dolomites. The oxygen, carbon and strontium isotope compositions suggest that this calcite cementation occurred from meteoric waters mixed with Burdigalian - Langhian marine waters trapped in the sediments and expelled by compaction in the moderate to deep burial realm. Normal faults were the conduits for upward migration of these fluids as well as for later oil expulsion from the Burdigalian - Langhian source rocks. Late corrosion associated with organic acid-enriched fluids took place prior or simultaneously to oil migration during the Pliocene, enhancing porosity and increasing reservoir quality.

KEYWORDS | **Casablanca oil field. Dolomite reservoir. Vug and fracture porosity. Diagenesis. Mediterranean Sea.**

INTRODUCTION

The Valencia Trough has been an oil-producing basin since 1970 when the first oil discovery was made (Amposta Marino C1 well). After many years of exploration, information has been published about geology and geodynamic evolution of the basin (*e.g.* Torres *et al.*, 1993; Roca, 1994), as well as on the petroleum system of the existing fields (*e.g.* Seemann *et al.*, 1990; Clavell and Berastegui, 1991; Varela *et al.*, 2005).

In the adjacent onshore areas of the Maestrat Basin (Iberian Ranges) and the Catalan Coastal Ranges, Upper Jurassic-Cretaceous limestones and dolomites stratigraphically equivalent to those constituting the main reservoir of the oil fields in the Spanish Mediterranean Sea have been the subject of numerous investigations. The thorough understanding of sedimentary and structural data (*e.g.* Salas *et al.*, 2001; Gaspar-Escribano *et al.*, 2004) as well as fluid circulation models proposed for onshore outcrops (*e.g.* Travé *et al.*, 1998; Travé and Calvet, 2001; Rossi *et al.*, 2001; Baqués *et al.*, 2011; Baqués *et al.*, 2012) have contributed to the general comprehension of the offshore evolution. However, there is a lack of information on porosity types, distribution, and their contribution to total reservoir porosity, fluid migration systems in the offshore areas, and diagenetic processes affecting oil fields in the Valencia Trough.

This study is focused on the Casablanca oil field, the largest producing field in the Valencia Trough. Development and production history of the field as well as geology and reservoir characteristics have been presented by Watson (1982), Orlopp (1988), Lomando *et al.* (1993) and Vallaure and Mallo-García (2005). However, little has been said about the mechanisms, age and consequences of the pervasive dolomitization affecting this field, or on the geochemical characteristics and evolution of the responsible fluids.

The goal of the present work is to reveal the diagenetic processes affecting reservoir rocks of the Casablanca oil field and the fluid migration history before and during main oil emplacement. For these purposes: i) diagenetic products are petrologically and geochemically characterized; ii) composition of the mineralizing fluids is defined; and iii) the diverse fluid flow events are attributed to most important tectonic phases affecting the north-eastern Iberian Peninsula.

GEOLOGICAL SETTING

The Casablanca oil field is located in the north-eastern part of the Valencia Trough, stretching between the Iberian Peninsula and the Balearic Promontory, at 45km offshore south-east of the city of Tarragona (Fig. 1A, B).

The Valencia Trough is a NE-SW orientated basin developed as a result of the extensional tectonic regime that affected the western Mediterranean during the Neogene (late Oligocene-Miocene). Owing to this rifting period a system of horsts, grabens and half-graben structures were formed. These extensional structures were controlled by ENE-WSW and NE-SW trending normal faults (Fig. 1C), resulting from the tectonic reactivation of previous compressive fractures formed during the regional Paleogene contraction (late Eocene - early Oligocene) (Roca, 1994; Cabrera *et al.*, 2004). The Catalan Coastal Ranges represent the northern boundary of the Valencia Trough, whereas the Betic thrust-and-fold belt front forms the southern boundary (Clavell and Berastegui, 1991).

The Casablanca oil field, about 1km wide and 11km long, is located in a structural high of Mesozoic carbonates. This paleohigh is bounded by faults along its northwestern and southeastern flanks (Lomando *et al.*, 1993).

The main reservoir rocks in the Casablanca oil field are Upper Jurassic and Lower Cretaceous shallow marine carbonates (limestones and dolostones). The onshore well-exposed outcrops provide detailed sections (Esteban, 1973; Salas, 1987; Nadal, 2001; Martín-Martín *et al.*, 2010). Part of the Valencia Trough and the present Catalan Coastal Ranges were uplifted during the Paleogene contraction (Roca, 1994; Gaspar-Escribano *et al.*, 2004). The Mesozoic carbonates (and probably Paleogene materials) were then exposed, eroded and karstified. Later, during the Miocene and due to the regional rifting stage, the compressional structures were overprinted by extensional faults giving rise to the NE – SW trending structures and the erosion and local karst rejuvenation of the Mesozoic carbonates in the developed structural highs (Roca, 1994; Gaspar-Escribano *et al.*, 2004; Varela *et al.*, 2005). Well-preserved examples of karstic sequences have been described onshore, in the Catalan Coastal Ranges (Esteban, 1973; Klimowitz *et al.*, 2005), where karst would probably be as old as Late Cretaceous (Esteban, 1991). Paleogene and Neogene karst successions can be distinguished in selected outcrops (Baqués *et al.*, 2011; Baqués *et al.*, 2012).

The transitional and marine Neogene sediments were deposited unconformably over the Mesozoic basement. The synrift sequence begins with the siliciclastic sediments of the Basal Tertiary Group (Fig. 2). These sediments are unconformably overlain by dark gray to black argillaceous limestone with variable organic-carbon content that constitute part of the Casablanca Group: the so-called Casablanca or Tarraco Formation (Fm.), deposited during the Burdigalian - Langhian (early to middle Miocene) in a restricted shelf environment. This formation is equivalent to the Alcanar Formation, which is the main source rock of the Casablanca oil field (Demaison and Bourgeois, 1984; Permanyer and Salas, 2005). The Casablanca Fm. is also thought to be the

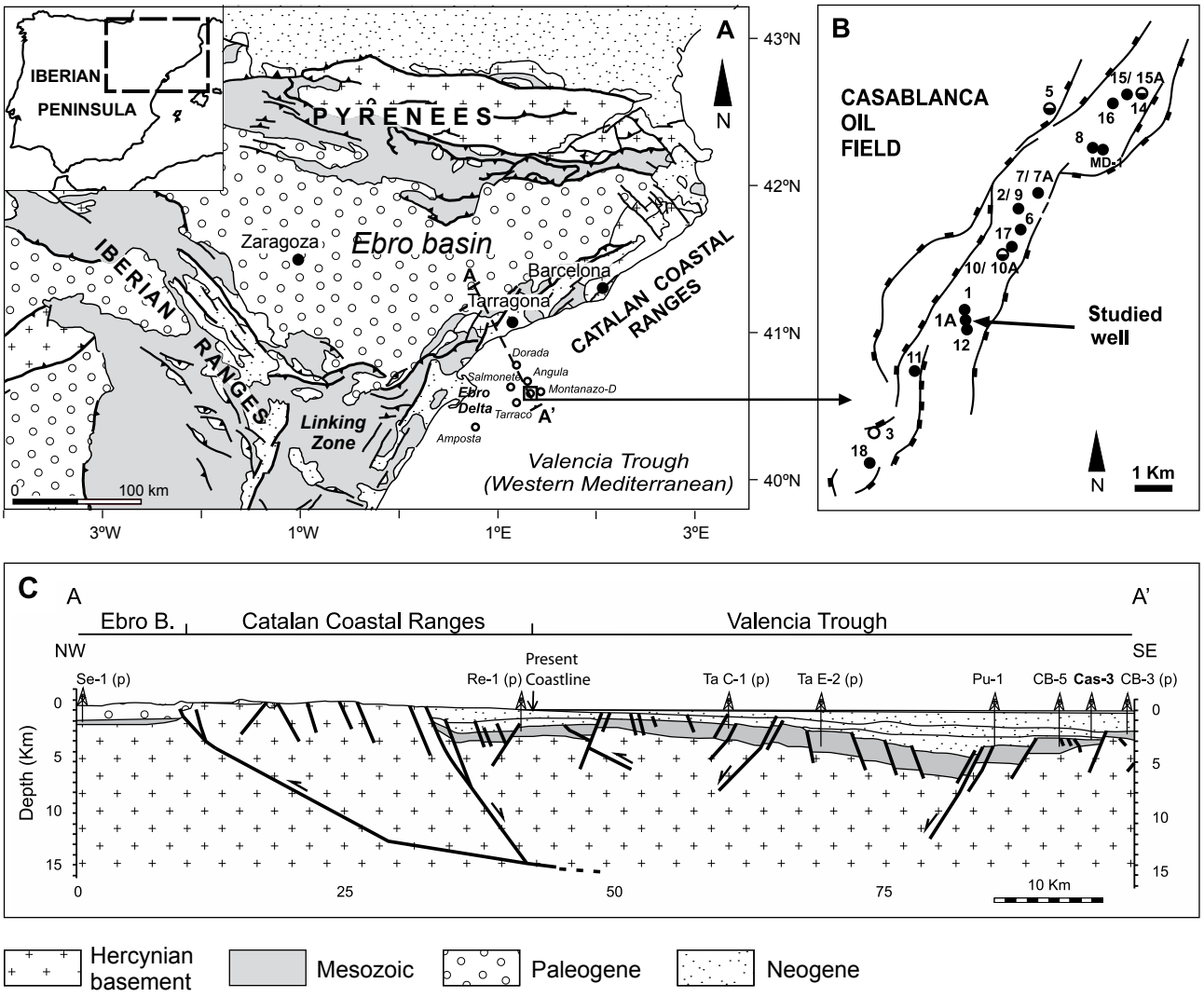

FIGURE 1 | A) Simplified geological map of the north-western Iberian Peninsula, with location of the main oil fields in the Valencia Trough. B) Enlarged area of the Casablanca oil field, showing location of the Casablanca-1A well (Lomando et al., 1993). C) Geological cross section of the Catalan Coastal Ranges and the Valencia Trough (Cabrera et al., 2004), location in (Figure 1A).

proximal seal, together with the Serravallian (middle Miocene) calcilutites and marls of the San Carlos Group. The regional seal is constituted by the Castellón Shale Fm. of the Castellón Group, which overlaps the underlying extensional structures and represents the beginning of the postrift sequence (Vallaure and Mallo-García, 2005).

The Casablanca-1A well

The Casablanca oil field is the largest producing field in the Spanish Mediterranean Sea. It was discovered in 1975 by CHEVRON and is still on production being Repsol, formerly ENIEPSA, the main operatorship.

The field is penetrated by more than 20 wells of which the Casablanca-1A well notably stands out for its good core recovery. Around 100 meters of Upper Jurassic carbonate reservoir are present in the Casablanca-1A well. The main features that characterize the dolomitized host rocks cored by this well are fracture and vug porosity, partly cemented and partly occluded by dolomitized reddish to brownish sediments. Lomando *et al.* (1993) also described several types of clast or matrix-supported breccias. The most important petrographic features identified in cores from Casablanca-1A well are represented in Figure 3.

METHODS

A total of thirty-one samples from Casablanca-1A well core between 2660 and 2760m (Fig. 3) were carefully studied in order to identify the diagenetic phases and their spatial

and temporal relations. Thirty-six stained thin sections were examined using optical and cathodoluminescence (CL) (Technosyn Cold Cathodoluminescence Model 8200 MkII, operating at 10-18kV gun potential and 400μm beam current) and photoluminescence microscopy (Nikon Optiphot, equipped with a blue-violet excitation fluorescence filter that covers an excitation wavelength range between 400-446nm). Nine samples were investigated to determine the morphology of the diagenetic products and study the texture and the qualitative chemical composition in major elements of the non-carbonate fraction by an environmental scanning electron microscope (ESEM Quanta 200 FEI, XTE 325/D8395) with an energy dispersive spectrometer (EDX), and equipped with backscatter image technology.

In order to analyze major, minor and trace element composition (Ca, Mg, Mn, Fe, Sr and Na) of the diagenetic products, eight C-coated polished thin sections were investigated. The analyses were performed using a CAMECA SX-50 electron microprobe, equipped with four vertically oriented WD X-ray spectrometers and operating at 20kV of excitation potential, 10µm of beam diameter

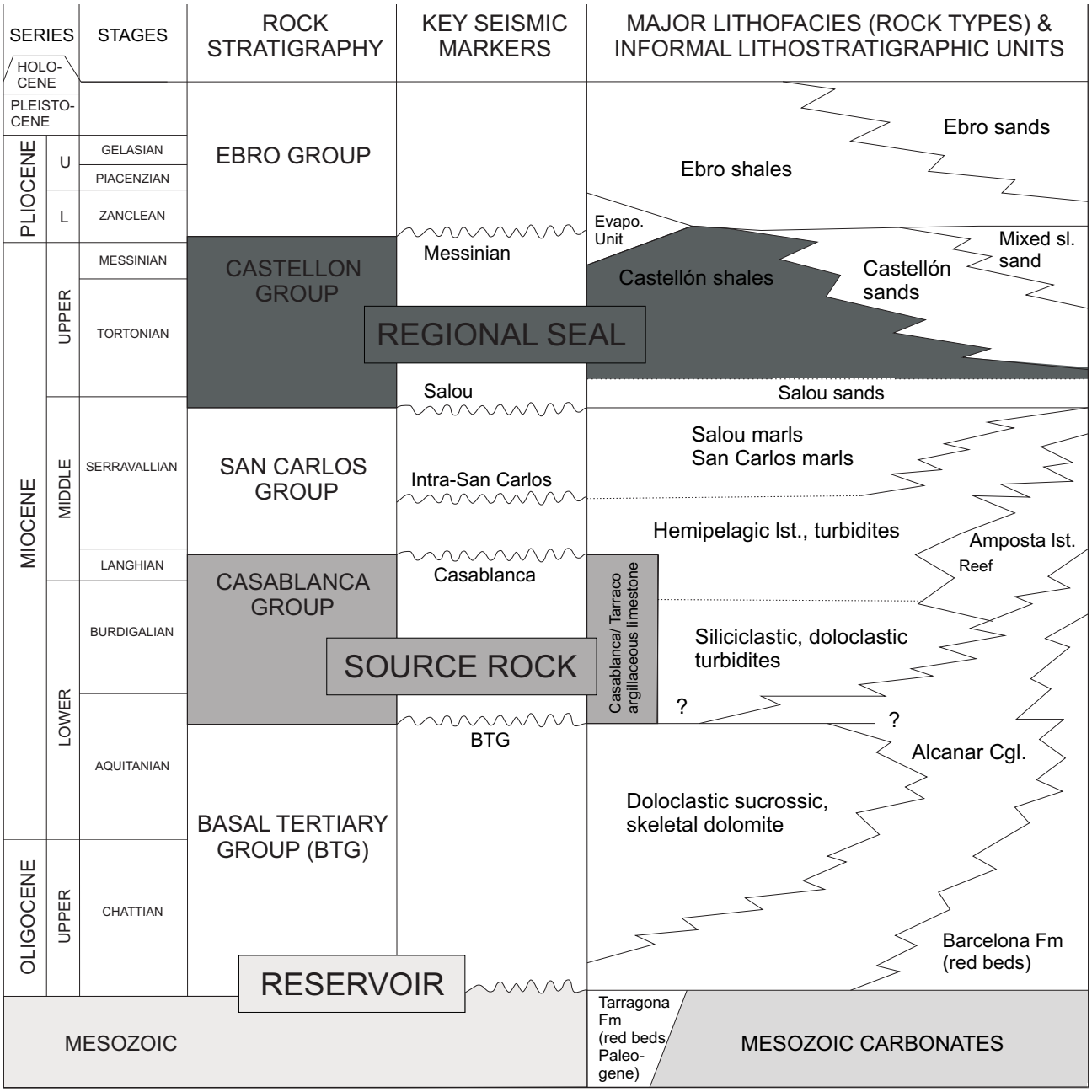

FIGURE 2 | Schematic stratigraphic chart of the Mesozoic and Neogene sediments in the Valencia Trough, indicating the stratigraphical position of the reservoir rock, source rock and regional seal rock (Esteban, 1998).

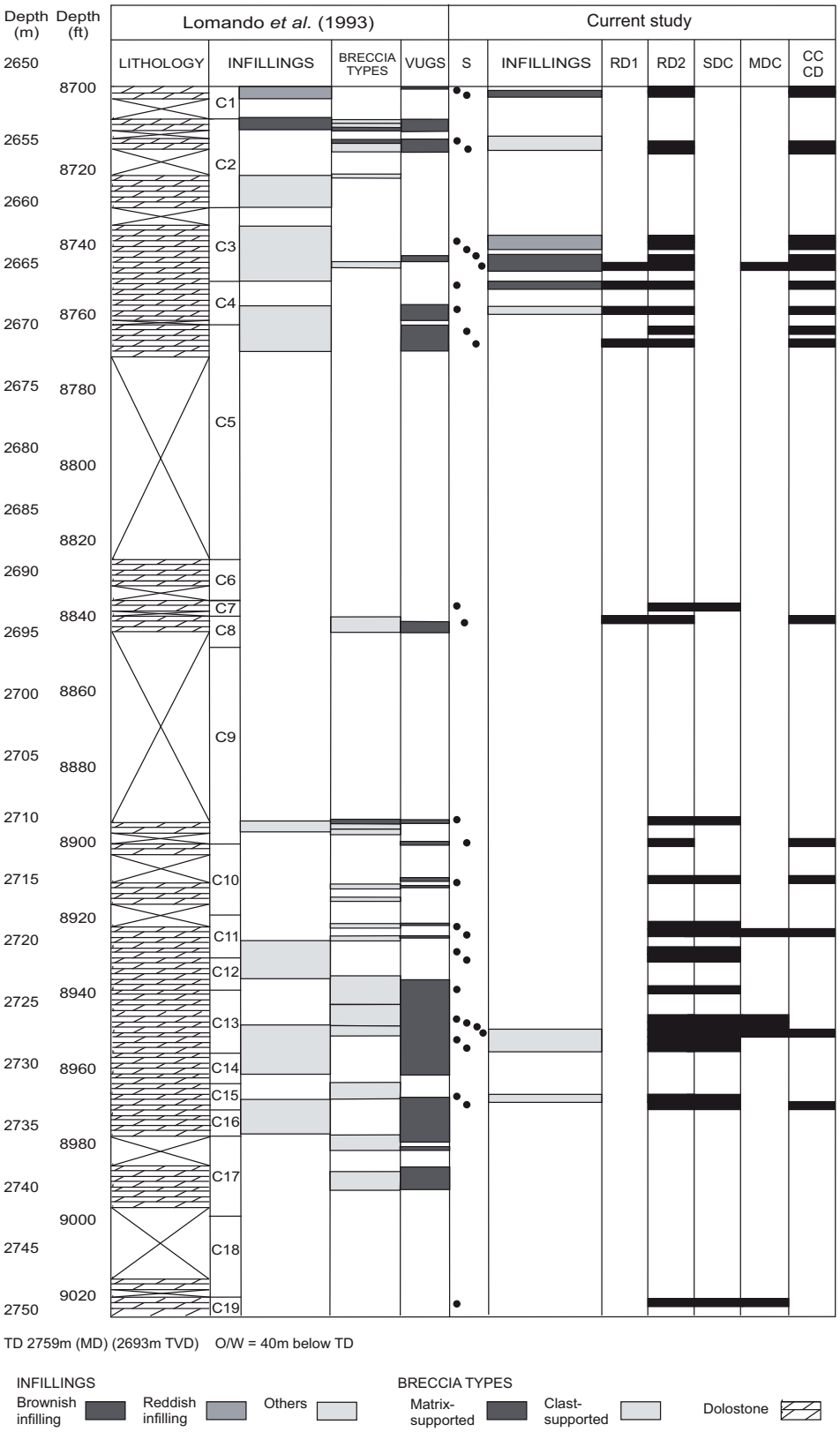

FIGURE 3 | Petrographic description of the Casablanca-1A well core, showing distribution in depth of the diagenetic products, and location of the studied samples. Lithology, infillings, breccia types and vug porosity columns according to Lomando et al. (1993). C: Cores; S: Samples; RD1: Replacive dolomite 1; RD2: Replacive Dolomite 2; SDC: Saddle Dolomite Cement; MDC: Milky-white Dolomite Cement; CC: Calcite Cement; CD: Calcitized Dolomite; TD: Total Depth; MD: Measured Depth; TVD: True Vertical Depth; O/W: oil-water contact.

and 10nA of current intensity for the Ca and Mg analyses, and 50nA for Mn, Fe, Sr and Na. The detection limits are 495ppm for Ca, 493ppm for Mg, 131ppm for Mn, 128ppm for Fe, 161ppm for Sr and 128ppm for Na. Na and Mn are mostly under the detection limit in all the identified diagenetic products. Standards used were calcite for Ca, periclase for Mg, albite for Na, celestite for Sr, iron oxide for Fe and rodonite for Mn. Precision on major element analyses averaged 6.86% standard error at 3σ confidence level. The stoichiometry of dolomites was calculated and expressed as mole percentage of $CaCO_3$.

Oxygen and carbon isotopes were measured on thirty-five pure dolomite and three pure calcite samples. 10-60μg of powdered samples were reacted with 103% H_3PO_4 for 3 and 15 minutes (calcite and dolomite, respectively) in vacuum at 70ºC. The evolved CO_2 was analyzed on a Thermo Electron (Finnigan) MAT-252 mass spectrometer. The values are reported in per mil with respect to the VPDB (Vienna Pee Dee Belemnite) standard, having a precision of ± 0.05‰ VPDB for $\delta^{18}O$ and ± 0.02‰ VPDB for $\delta^{13}C$.

For $^{87}Sr/^{86}Sr$ ratio analyses, four powdered carbonate samples (3 dolostones and 1 calcite cement) were converted to chlorides by leaching them firstly in acetic acid 10% in and later in HCl 2.5N. The final liquid samples were loaded into a chromatographic column with DOWEX 50Wx12 200/400 mesh cation exchange resin. A VG Sector 54 TIMS mass spectrometer was employed to analyze the isotopic composition of the isolated Sr. Results were controlled by repetitive analysis of the NBS-987 standard, averaging (n= 11) 0.710202 ± 0.00004 (2σ). All results were normalized to $^{87}Sr/^{86}Sr$= 0.1194. Analytical error is 0.01% (2σ).

The study of the non-carbonate fraction was performed by leaching powdered bulk rock samples in HCl 10% in volume at room temperature to remove the carbonates. The bulk mineralogy and clay mineral composition of the non-carbonate fraction were then analyzed by X-ray diffraction as randomly oriented powder and oriented preparations (air-dried, glycolated and heated at 550ºC), respectively, in a Siemens D-500 diffractometer. The morphology of minerals in the non-carbonate fraction was characterized by a Jeol JEM 1010 transmission electron microscopy (TEM). The strontium isotopic signal of the clay fraction was also obtained; the residue of the carbonate leaching (acetic acid 10% in and later HCl 2.5N attacks) was dissolved with a mixture of HF and HNO_3 at 120ºC for 48 hours. After evaporation, the solid was redissolved in HNO_3 to avoid fluorine compounds and dried again. Final dissolution was reached several times with HCl 6N and 2.5N and loaded into a chromatographic column.

PETROLOGICAL AND GEOCHEMICAL RESULTS

Because of the pervasive and fabric destructive dolomitization process, no clues of the original limestone fabric were observed in the Casablanca-1A well core. However, based on the study of other core wells from the Casablanca oil field, Watson (1982) described the original limestone as mudstones with scarce fossils, and skeletal wackestones and packstones with almost negligible primary porosity (ranging from 1 to 3%). According to the aforementioned author, the limestone penetrated by the Casablanca-1A well is Upper Jurassic (Kimmeridgian) in age.

The study of the 2660 to 2760m core range enables the identification of four types of dolomites, one type of calcite cement and one type of calcitized dolomite. Their petrological characteristics are summarized in Table 1. Figure 3 shows the distribution in depth of the different diagenetic products. Dolomite textures are reported using the terminology of Sibley and Gregg (1987). Major and minor and trace element and stable and radiogenic isotope data for each diagenetic phases are given in Table 2. Stable and radiogenic isotope results for individual samples are listed according to depth in Table 3 for C and O, and in Table 4 for Sr.

Replacive dolomite 1 (RD1)

Replacive dolomite 1 forms fine-sized (10-80μm) planar-s crystals that replace the original limestone and give rise to a sucrosic fabric. It appears as centimetric-scale isolated patches within replacive dolomite 2 (RD2) crystal mosaics. The crystals are cloudy under optical microscope with patchy bright red color in CL (Fig. 4, 5 and 6). RD1 is characterized by Fe content from 2514 to 2950ppm and Sr content from 397 to 479ppm. The $\delta^{18}O$ range from -10.8 to -7.6‰ VPDB and the $\delta^{13}C$ ranges from +1.1 to +1.7‰ VPDB (Fig. 7). RD1 crystals are non-stoichiometric, with $CaCO_3$ ranging between 56.46 and 57.76 mole % (Fig. 8).

Replacive dolomite 2 (RD2)

Replacive dolomite 2 (RD2) accounts for approximately 90% by volume of the studied rock core samples. RD2 forms fine- to coarse-sized crystals (20-500μm) that replace RD1 and carbonate infillings in fracture and in vug porosity.

RD2 dominantly forms planar-s crystals showing turbid (inclusion-rich) centers and clear (inclusion-poor) borders. These borders display a dull red cathodoluminescence color, whereas the crystal centers often contain relicts of the precursor RD1 with its characteristic bright CL color (Figs. 4; 5). Less frequently, RD2 forms planar-s to planar-e

crystals that replace the carbonate fraction infilling fracture and vug porosity (karst infillings). Crystal borders are moderately corroded and occasionally show bright orange luminescence rims (Fig. 5, 6). The karst infillings are exclusively identified in the samples from the upper part of the studied well (last 15m), and are clearly distinguished from the host dolostone on the basis of their brown and red coloring (Fig. 4). Typically these infillings contain from 2 to 9% of non-carbonate fraction (see Non-carbonate minerals section). Occasionally, RD2 also forms limpid planar-e crystals that cement fractures. These crystals exhibit the characteristic dull red CL color and the partially corroded borders reported above (Fig. 5).

The $\delta^{18}O$ values range from -10.4 to -2.3‰ VPDB and the $\delta^{13}C$ ranges from +0.95 to +2.4‰ VPDB (Fig. 7). Stoichiometry of the RD2 crystals ranges from 54.43 to 57.78 mole % CaCO3, (Fig. 8). RD2 has variable Fe and Sr content ranging from below detection limit to 8341ppm, and from below detection limit to 677ppm, respectively. The $^{87}Sr/^{86}Sr$ value ranges from 0.708607 to 0.709202 (Fig. 9).

Saddle dolomite cement (SDC)

Saddle dolomite cement forms fine- to very coarse-sized (100μm to 1.4mm long; 50μm to 2 mm wide) non-planar crystals characterized by curved crystal faces and undulatory extinction under cross polarized light. Saddle dolomite cement has turbid centers, corresponding to the replacive dolomite 1 and clear (inclusion-poor) and dull luminescent overgrowth (Figs. 4; 5). Saddle dolomite cement commonly occlude fracture and vug porosity and show partially corroded crystal borders. It is characterized by Fe content below detection limit and Sr values ranging from 261 to 565ppm. The $\delta^{18}O$ values of this dolomite cement range from -8.9 to -6.8‰ VPDB, and the $\delta^{13}C$ range from +1.5 to +2.5‰ VPDB (Fig. 7). Saddle dolomite cement is non-stoichiometric, ranging from 54.64 to 55.32 mole% $CaCO_3$ (Fig. 8; Table 2).

Milky-white dolomite cement

Milky-white dolomite cement forms fine- to medium-sized (40-150μm) planar-s to non-planar crystals that fill fractures as a single phase or after partial saddle dolomite cementation. Milky-white dolomite cement crystals show milky white color under the optical microscope, being non-luminescent in cathodoluminescence (Figs. 4; 5). Milky-white dolomite cement yields the highest Fe and Sr content of all the studied dolomites, having Fe and Sr contents from below detection limit to 13027ppm, and from 371 to 684ppm, respectively. The $\delta^{18}O$ values are from -11.9 to -11.4‰ VPDB, and the $\delta^{13}C$ from +1.0 to +1.2‰ VPDB (Fig. 7). Milky-white dolomite cement has the most variable stoichiometry with values between 53.34 and 58.36 mole % $CaCO_3$ (Fig. 8).

Calcite cement and calcitized dolomite

The post-dolomitization sequence included precipitation of calcite cement and partial calcitization of dolomite. The calcite cement has limpid, equant, coarse-sized (400μm to 4mm) crystals that form an equigranular blocky mosaic. It fills fracture, vug and intercrystalline porosity remaining after saddle dolomite cement and milky-white dolomite cement precipitation (Figs. 4; 6). Calcite cement shows dull dark red luminescence color under cathodoluminescence (Fig. 5). It has a Fe content ranging from 216 to 2922ppm, and Sr content ranging from 222 to 1149ppm. The $\delta^{18}O$ ranges from -14.3 to -13.1‰ VPDB,

TABLE 1 | Main petrographic features of dolomites, calcitized dolomite and calcite cement identified in the Casablanca-1A well core

Description	RD1	RD2	RD2 (karstic infillings)	RD2 (cement)	SDC	MDC	CC	CD
Type and occurrence	Replacive, affecting the original limestone	Replacive, affecting Dolomite 1	Replacive, affecting infillings in fracture and vug porosity	Cement, occluding fracture porosity	Saddle dolomite cement, occluding fracture and vug porosity	Cement, occluding fracture porosity	Cement, occluding fracture, vug and intercrystalline porosity	Affecting cloudy centers and rhomb-shaped crystalline rims
Fabric and texture	Destructive and pervasive; Hipidiotopic mosaic	Pervasive and highly destructive; Hipidiotopic mosaic	Selective; Idiotopic mosaic	Cement	Cement	Cement	Cement. Equant mosaic	Selective
Crystal shape	Planar-s	Planar-s	Planar-e	Planar-e	Curved crystal faces (non-planar)	Planar-s to non-planar		Euhedral and rhomb-shaped
Crystals size	Fine-sized (10-90µm)	Fine to medium-sized (20-140µm)	Fine- to coarse-sized (40-450µm)	Fine- to coarse-sized (50-500µm)	Fine- to coarse-sized (100µm–1.4mm long; 50µm–2mm wide)	Fine- to medium-sized (40–150µm)	Coarse-sized (400µm-4 mm)	Fine to coarse-sized (5-500µm)
Color	Dirty	Cloudy centers and clear rims	Cloudy centers and clear rims	White	Cloudy centers and clear rims	Milky white	White	White
CL	Non-homogeneous bright red	Rim: dull red Center: Dolomite 1	Dull red Occasionally, bright orange rims	Dull red	Rim: dull red Center: non-luminescent	Non-luminescent	Dull dark red	Dull dark red

TABLE 2 | Major, minor and trace element composition, mole % of $CaCO_3$, oxygen and carbon isotope composition, and strontium isotope composition of dolomites, calcitized dolomite and calcite cement identified in the Casablanca-1A well core. It is included the calculated Mg/Ca, Sr/Ca and Ca/Fe molar ratios of the calcite parent fluid, applying the distribution coefficient equation in McIntire, 1963, and the strontium isotope composition of the associated clays. < d.l. = below detection limit; n = number of samples; - = not analyzed. a) Using K_{Mg}= 0.1163 (at 90ºC) (Katz, 1973); b) Using K_{Sr}= 0.06 (at 25, 40, 98 and 200ºC) (Katz *et al.*, 1972; Stoessell *et al.*, 1987); c) Using K_{Fe}= 5 (Dromgoole and Walter, 1990)

Description		RD1	RD2	RD2 (karstic infillings)	RD2 (cement)	SDC	MDC	CC	CD
Na (ppm)	Max.	326	689	294	329	174	202	280	231
	Min.	194	< d.l.	< d.l.	< d.l.	< d.l.	< d.l.	< d.l.	< d.l.
	Mean	266	-	-	-	-	-	-	-
Mg (ppm)	Max.	122215	128604	122661	127156	130134	126277	6519	15746
	Min.	118742	118800	119000	117600	123872	117022	1500	2971
	Mean	120659	124515	122545	122941	127280	123962	4231	6926
Ca (ppm)	Max.	230742	228511	227450	231010	226826	230241	404600	398839
	Min.	223300	217906	215950	218151	214834	212624	388400	376956
	Mean	226092	222566	222313	224479	222030	220004	395579	391506
Mn (ppm)	Max.	< d.l.	< d.l.	450	164	< d.l.	< d.l.	324	397
	Min.	< d.l.	< d.l.	< d.l.	< d.l.	< d.l.	< d.l.	< d.l.	< d.l.
	Mean	-	-	-	-	-	-	-	-
Fe (ppm)	Max.	2950	8341	7051	5993	< d.l.	13027	2922	763
	Min.	2514	< d.l.	1959	849	< d.l.	510	216	351
	Mean	2701	-	3496	2911	-	5006	1555	547
Sr (ppm)	Max.	479	677	672	591	565	684	1149	1149
	Min.	397	< d.l.	< d.l.	< d.l.	261	317	222	598
	Mean	452	-	-	-	396	424	520	827
mole% $CaCO_3$	Max.	57.76	56.90	57.29	57.78	55.32	58.36	99.23	98.62
	Min.	56.46	54.43	54.69	54.84	54.64	53.34	97.20	94.22
	Mean	56.90	55.87	56.11	56.37	55.54	55.45	98.23	97.18
n		3	30	34	16	20	11	25	34

Description			RD1	RD2	RD2 (karstic infillings)	RD2 (cement)	SDC	MDC	CC	CD
Molar ratio Mg/Ca fluid [a]	n=23	Max.	-	-	-	-	-	-	0.24	-
		Min.	-	-	-	-	-	-	0.05	-
		Mean	-	-	-	-	-	-	0.14	-
Molar ratio Sr/Ca fluid [b]	n=23	Max.	-	-	-	-	-	-	0.021	-
		Min.	-	-	-	-	-	-	0.004	-
		Mean	-	-	-	-	-	-	0.013	-
Molar ratio Ca/Fe fluid [c]	n=23	Max.	-	-	-	-	-	-	514	-
		Min.	-	-	-	-	-	-	38	-
		Mean	-	-	-	-	-	-	276	-
$\delta^{18}O$ (‰ VPDB)		Max.	-7.6	-6.8	-6.1	-	-7.2	-11.4	-13.1	-
		Min.	-10.8	-10.4	-9.6	-	-8.9	-11.9	-14.3	-
		Mean	-9.2	-9.0	-7.6	-	-8.0	-11,7	-13.7	-
$\delta^{13}C$ (‰ VPDB)		Max.	+1.7	+1.3	+1.4	-	+2.5	+1.2	-0.2	-
		Min.	+1.1	+1.0	+1.0	-	+1.5	+1.0	-0.4	-
		Mean	+1.3	+1.1	+1.2	-	+2.0	+1.1	-0.3	-
n			4	8	15	-	5	3	3	-
$^{87}Sr/^{86}Sr$ ± standard error			-	0.708607 ± 7	0.709137 ± 6 0.709202 ± 5	-	-	-	0.708521± 7	-
$^{87}Sr/^{86}Sr$ ± standard error Associated clay minerals			-	0.765469 ± 11	0.724652 ± 8 0.732111 ± 15	-	-	-	-	-
n			-	1	2	-	-	-	1	-

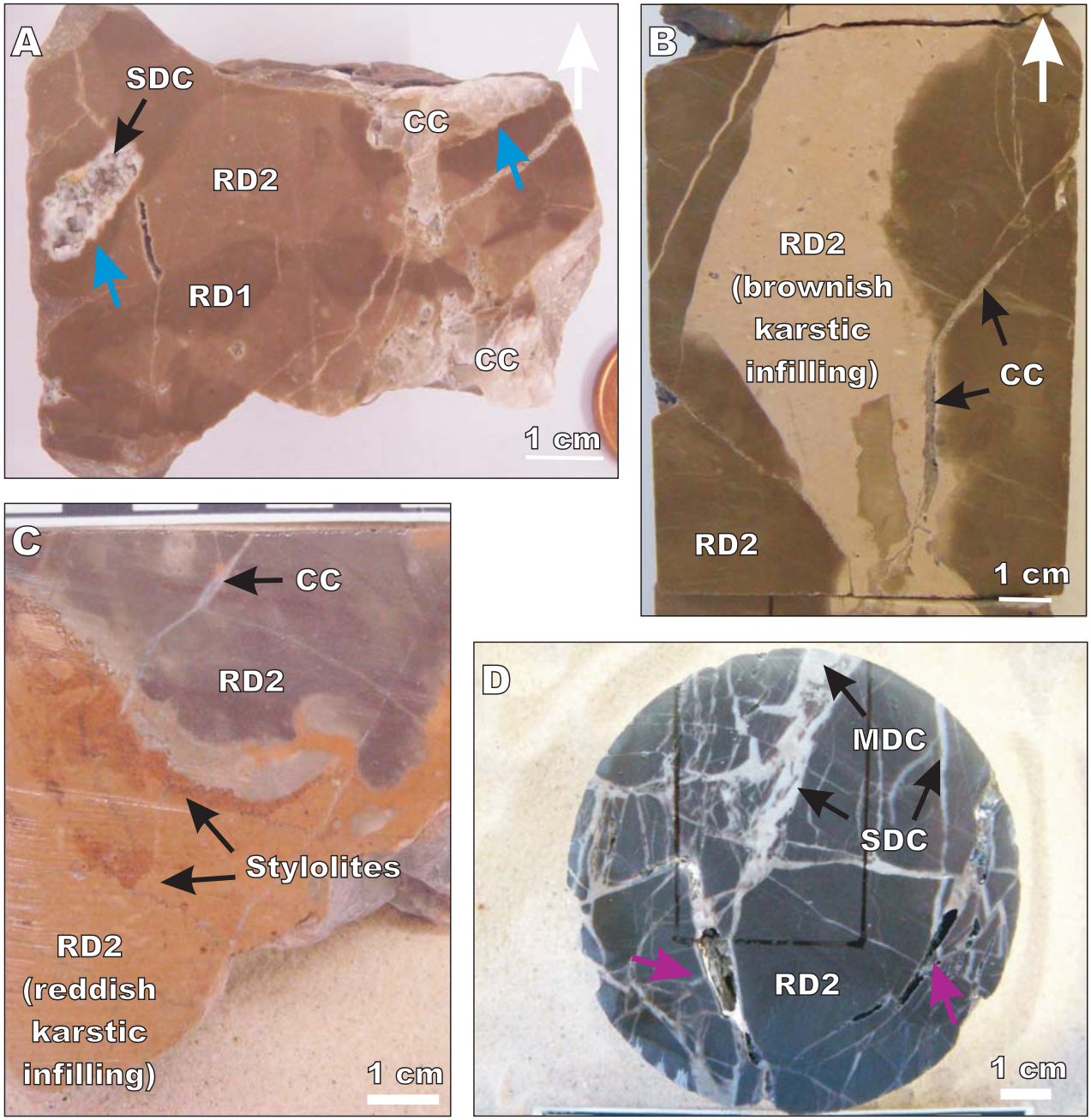

FIGURE 4 | Photographs of representative hand-samples of the Casablanca-1A well core, illustrating the distribution and relationships of the identified diagenetic products. White arrows indicate sample orientation; blue arrows indicate vug porosity; purple arrows indicate partially open fractures. Samples (from A to D): RM-30, RM-32, RM-47, RM-44. RD1: Replacive Dolomite 1; RD2: Replacive Dolomite 2; SDC: Saddle Dolomite Cement; MDC: Milky-white Dolomite Cement; CC: Calcite Cement.

and the $\delta^{13}C$ oscillates between -0.4 and -0.2‰ VPDB (Fig. 7). A single $^{87}Sr/^{86}Sr$ ratio gave a value of 0.708521 (Fig. 9).

Calcitization of dolomite affects all previously described dolomites to a greater or lesser extent. Dissolution and replacement partially affects the turbid centers and the thin, rhomb-shaped crystalline rims of dolomite crystals (Fig. 5 and 6). Calcitized dolomite crystals have a dull dark red cathodoluminescence color, similar to that shown by the calcite cement. Calcitized dolomites have Fe content ranging from 351 to 763ppm, and Sr content ranging from 598 to 1149ppm.

The calcite cement, as well as all dolomite stages, was cut by closed subvertical and subhoritzontal stylolites (Fig. 4). Chronological relations between subvertical and subhoritzontal stylolites have not been established.

Non-carbonate minerals

Clay minerals and iron sulfides, together with minor quartz, barite, K-feldspar, ilmenite, Ti oxides (rutile and anatase) and Fe oxides, constitute the non-carbonate fraction within RD2 crystal mosaics. These non-carbonate minerals are more abundant in RD2, occupying vug and fracture porosities (between 2 and 9%), than in RD2 replacing the host rock (up to 1%).

Two types of illitic particles were recognized in close association with the dolomitized host rock, and the fracture and vug infillings (Fig. 6): i) clay minerals with pseudohexagonal, flaky shape and irregular crystal edges that uniformly coat RD2 crystals; and ii) clay minerals with fibrous crystal habit usually showing honeycomb texture. X-ray diffraction (XRD) analyses, supported by energy dispersive X-ray (EDX) analyses, evidence the presence of illite and mixed-layer illite-smectite (I/S). The Sr

TABLE 3 | Oxygen and carbon isotope results of individual samples analyzed in the Casablanca-1A well core

Description	Depth (m)	Sample	$\delta^{18}O$ VPDB (‰)	$\delta^{13}C$ VPDB (‰)
RD1	2669.31	RM-20.1	-8.8	+1.2
	2694.3	RM-30.3	-7.6	+1.7
	2694.3	RM-30.4	-9.7	+1.1
	2655-2670	RM-47.4	-10.8	+1.2
RD2	2652.06	RM-12.2	-10.4	+1.1
	2655.59	RM-13.2	-6.8	+1.9
	2664.48	RM-16.2	-9.8	+1.0
	2666.26	RM-32.3	-8.9	+1.2
	2693.69	RM-24.3	-9.4	+2.0
	2694.3	RM-30.2	-10.3	+1.0
	2720.05	RM-29.4	-6.9	+2.4
	2655-2670	RM-47.3	-9.3	+1.1
RD2	2652.06	RM-12.1	-6.1	+1.3
(karstic infillings)	2652.06	RM-12.4	-6.3	+1.3
	2655.59	RM-13.1	-7.73	+1.11
	2666.26	RM-32.1	-6.8	+1.1
	2666.26	RM-32.2	-6.8	+1.1
	2666.26	RM-31.1	-6.5	+1.0
	2666.87	RM-19.4	-2.3	+1.4
	2664.49	RM-16.1	-8.3	+1.2
	2664.49	RM-16.5	-8.3	+1.2
	2664.74	RM-17.2	-9.3	+1.1
	2664.74	RM-17.6	-9.6	+1.1
	2655-2670	RM-47.1	-7.0	+1.1
	2655-2670	RM-47.2	-7.2	+1.1
	2655-2670	RM-46.1	-7.4	+1.2
	2694.3	RM-30.5	-9.10	+0.95
SCD	2693.69	RM-24.1	-8.8	+2.2
	2693.69	RM-24.2	-8.9	+2.2
	2720.05	RM-29.1	-6.8	+1.8
	2727.52	RM-37.1	-7.2	+2.5
	2734.84	RM-44.2	-8.3	+1.5
MDC	2720.05	RM-29.2	-11.9	+1.0
	2720.05	RM-29.3	-11.9	+1.2
	2734.84	RM-44.1	-11.4	+1.2
CC	2656.05	RM-15.2	-13.1	-0.4
	2664.74	RM-17.1	-14.3	-0.3
	2671.14	RM-22.1	-13.8	-0.2

TABLE 4 | Strontium isotope results of individual samples analyzed in the Casablanca-1A well core

Description	Depth (m)	Sample	$^{87}Sr/^{86}Sr$
RD2	2666.26	RM-32b	0.708607 ± 7
RD2 (karstic infillings)	2666.26	RM-32a	0.709202 ± 5
	2655-2670	RM-47a	0.709137 ± 6
CC	2655-2670	RM-47b	0.708521 ± 7
Clay minerals associated to RD2	2666.26	RM-32b	0.765469 ± 11
Clay minerals associated to RD2	2666.26	RM-32a	0.732111 ± 15
(karstic infillings)	2655-2670	RM-47a	0.724652 ± 8

isotopic ratios of the clay mineral fraction range between 0.724652 and 0.765469 (Table 4).

Scattered irregular pyrites (<10μm) occur within RD1 and replacive dolomite 2 crystal mosaics. Locally, pyrite also fills corroded growth zones (± cleavages) of replacive dolomite 2 crystals (Fig. 6).

Porosity types

The primary porosity of the original limestone was entirely obliterated by dolomitization and cementation processes. The porosity responsible for reservoir quality of this well is therefore of secondary origin and comprises vug, fracture and intercrystalline types. Minor amounts of moldic porosity, after partial dolomite crystal dissolution, are also present. The average porosity of the oil saturated zone in Casablanca core wells was estimated between 7 and 12% of the total rock volume. It means an increase up to 9% with respect to the initial porosity of the limestone rock (Watson, 1982).

Vug porosity forms irregular shaped cavities, up to 2cm in size, totally occluded or geopetally lined by the dolomitized brownish and reddish karstic infillings (replacive dolomite 2), as well as by saddle dolomite cement or calcite cement (Figs. 4; 5; 6). Vugs are oil impregnated, as evidence photoluminescence analysis, and commonly linked to open fractures.

Fracture porosity consists of vertical to subvertical fractures partially or totally cemented (saddle dolomite cement, milky-white dolomite cement and CC) and/or occluded by dolomitized infillings (replacive dolomite 2) (Figs. 4; 5). The remaining porosity frequently contains oil.

Euhedral crystal mosaic of replacive dolomite 2 develops significant intercrystalline porosity (Fig. 5). This porosity is observed heavily impregnated by oil, especially when it is related to the dolomitized sediments infilling vug porosity (Fig. 6).

SYNTHESIS AND DISCUSSION

Uplift and subaerial exposure

Karstification of the Casablanca reservoir rocks generated vug porosity, enhanced fracture porosity and gave rise to some distinctive lithofacies such as the carbonate infillings occluding fracture and vug porosity. A karstic detrital origin of the infillings is supported by: i) illitic clay coatings; ii) geopetal distribution of some infillings; iii) the increase of non-carbonate fraction in the infillings with respect to the host dolostones; and iv) the presence of irregular pyrites, quartz and K-feldspar particles.

The presence of illitic minerals with irregular edges and flaky morphology that uniformly coat the dolomite crystals is commonly interpreted as detrital textures (*e.g.* Clauer and Chaudhuri, 1995; Clauer *et al.*, 2008). Similar textures observed in fluvial sandstones have been reported to result from mechanical infiltration of muddy materials (clays) within the alluvium (Moraes and De Ros, 1990). The delicate habit of the fibrous illitic material with a honeycomb texture, most likely I/S clays suggests a partial recrystallization of the clay coatings during subsequent burial (Sant'Anna *et al.*, 2006; Clauer *et al.*, 2008).

The carbonate infillings are interpreted as sediment derived from the erosion of the host limestones and other lithologies outcropping in the proximity of the study area. Similar red to green carbonate sediments to those investigated in this study, filling fracture and vug porosity in fractured and karstified dolostones, have been previously reported in the Casablanca oil field (Lomando *et al.*, 1993). The karstic origin of this vug porosity is widely accepted (Watson, 1982; Orlopp, 1988; Clavell and Berastegui, 1991). Karstification was related to the regional Paleogene contraction (Fig. 10B), which caused uplift, fracturing, subaerial exposure and intense weathering of the Mesozoic limestones (Varela *et al.*, 2005). Karstification prevailed until the Neogene extension (Fig. 10C), as evidenced in onshore outcrops (Baqués *et al.*, 2011; Baqués *et al.*, 2012) and in the Amposta oil field (Playà *et al.*, 2010).

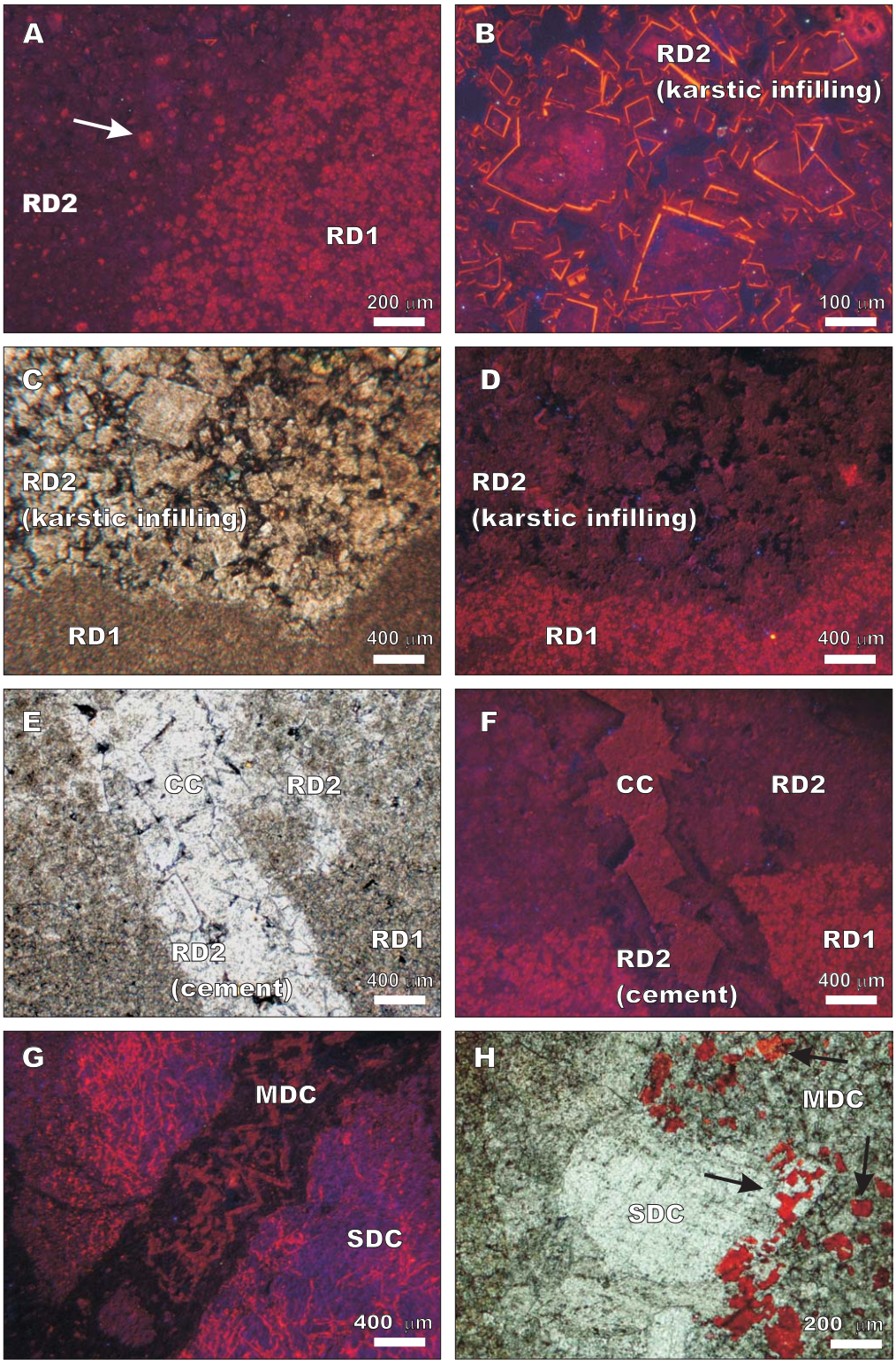

FIGURE 5 | Thin-section photomicrographs of the diagenetic products. A) Cathodoluminescence image showing the host rock, replaced by RD1 and RD2. Some crystals of RD2 display centers of the precursor bright red luminescent RD1 (arrow). Sample: RM-47. B) Cathodoluminescence image of RD2 replacing carbonate karst infillings showing dull red cathodoluminescence color with bright orange luminescent rims. Sample: RM-47. C) and D) Plane-polarized light and cathodoluminescence images, respectively, showing vug porosity filled with dull red luminescent RD2. Sample: RM-30. E) and F) Plane-polarized light and cathodoluminescence images, respectively, showing the spatial relation between RD1 and RD2. CC fills the remaining fracture porosity after RD2 cementation. Sample: RM-30. G) Cathodoluminescence image showing the spatial relation between SDC and MDC. Sample: RM-44. H) Plane-polarized light photomicrograph showing calcitization of SDC and MDC (arrows). Sample: RM-29. RD1: Replacive dolomite 1; RD2: Replacive Dolomite 2; SDC: Saddle Dolomite Cement; MDC: Milky-white Dolomite Cement; CC: Calcite Cement

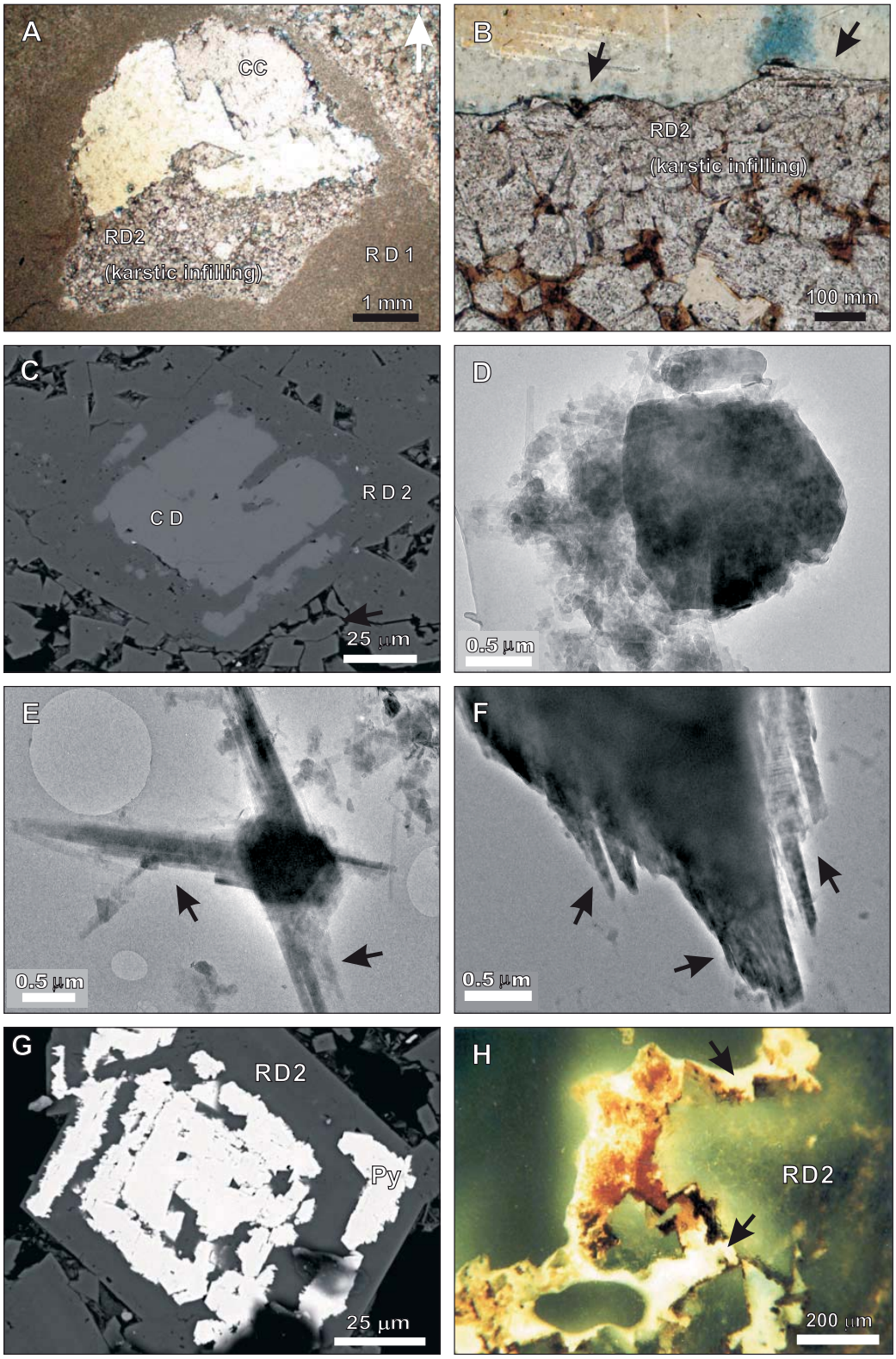

FIGURE 6 | Thin-section photomicrographs under optical (A, B), scanning electron (C, G), transmission electron (D, E, F) and photoluminescence (H) microscopes. A) Vug porosity partially filled by RD2 and CC, with geopetal distribution. White arrow indicates sample orientation. Sample: RM-30. B) Partially corroded RD2 crystals filling vug porosity. Sample: RM-13. C) Selective calcitization of centers and borders of RD2. Sample: RM-47. D) Illitic particle with pseudohexagonal shape and irregular crystal edges. Sample: RM-32. E) Illitic particle with fibrous crystal habit. Sample: RM-47. F) Recrystallization detail of an illitic particle arrows. Sample: RM-47. G) Pyrite crystals occluding corroded growth zones. Sample: RM-47. H) Photoluminescence photomicrograph showing oil within intercrystaline porosity in RD2 (arrows). Sample: RM-23. RD1: Replacive dolomite 1; RD2: Replacive dolomite 2; CC: Calcite cement; CD: Calcitized dolomite; Py: Pyrite.

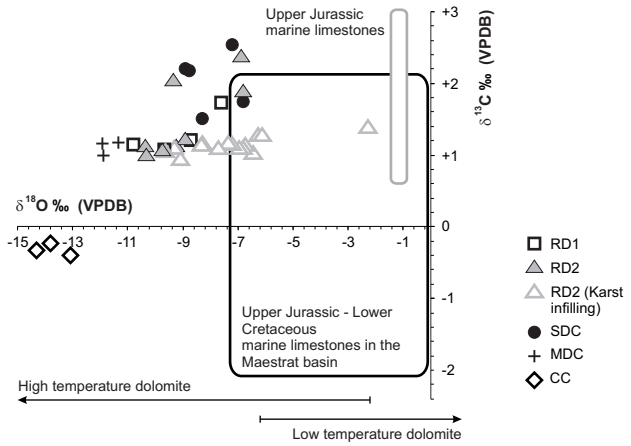

FIGURE 7 | Oxygen and carbon isotope composition of dolomites and the calcite cement identified in the Casablanca-1A well core. Range of values for Upper Jurassic marine limestones are according to Allan and Wiggins (1993). Range of values for Upper Jurassic - Lower Cretaceous marine limestones in the Maestrat basin (Iberian Chain) are according to Nadal (2001). $\delta^{18}O$ ranges for high and low temperature marine dolomites are based on a compilation from Allan and Wiggins (1993).

Dolomitization of the host rock

Petrological observations indicate that the original limestone fabric was obliterated by dolomitization in the studied core samples, although its preservation in nearby areas penetrated by other wells has been proved. The replacement of the host limestone gave rise to the fine-grained and dense sucrosic fabric of replacive dolomite 1 which is only preserved as centimetric isolated patches within replacive dolomite 2 crystal mosaic (Fig. 10). The presence of abundant cloudy replacive dolomite 1 relicts within the core of replacive dolomite 2 crystals is typically regarded as a recrystallization-related fabric (Nielsen *et al.*, 1994; Machel, 1997, 2004). Petrographic evidence of recrystallization is also indicated by the coarsening of replacive dolomite 2 crystal size compared to replacive dolomite 1 (Gregg, 2004; Machel, 2004). replacive dolomite 1 and replacive dolomite 2 present planar-s, locally planar-e, crystal boundaries indicating Formation. temperatures around 60ºC (the critical roughening temperature of dolomite according to Gregg and Sibley, 1984).

The $\delta^{13}C$ values of the replacive dolomite 1 and replacive dolomite 2 are very similar (Fig. 7), being within the range of Upper Jurassic marine limestones ($\delta^{13}C$ values between +0.6 and +3‰ VPDB; Allan and Wiggins, 1993). The oxygen isotope composition of replacive dolomite 1 and replacive dolomite 2 is notably depleted in relation to the standard $\delta^{18}O$ values of the Upper Jurassic marine limestones (from -1.3 to -1‰ VPDB; Allan and Wiggins, 1993). These values also fall outside the range of the Upper Jurassic Lower Cretaceous marine limestones outcropping in the onshore Maestrat Basin (southern Iberian Chain, eastern Spain), which range between -7.3 and -0.1‰ VPDB (Nadal, 2001; Fig. 7). Moreover, the partial overlapping between replacive dolomite 1 and replacive dolomite 2 signature suggest that both formed at similar temperature, suggesting that were partially cogenetic (Lonnee and Machel, 2006). Whereas the carbon isotope values of replacive dolomites are highly influenced by the pre-existing host carbonate, the oxygen isotopic composition reflects the Formation. temperature and the composition of the parent fluid (Land, 1980; Allan and Wiggins, 1993; Rameil, 2008).

Similarly, the carbonate fraction filling the fracture and vug porosity was also replaced during this dolomitization event, producing subhedral-euhedral, fine to coarse dolomite crystals (replacive dolomite 2 crystals, some with replacive dolomite 1 centers). The increase in crystal size entailed the Formation. of intercrystalline porosity, describing a tetrahedral to polyhedral pore system (Fig. 10D-2). This new intercrystalline porosity presumably increased the permeability of the rock (Warren, 2000).

The $^{87}Sr/^{86}Sr$ ratio of the host RD2 (0.708607 — 0.709202) is higher than that of Upper Jurassic marine water (0.7068 — 0.7072, Jones *et al.*, 1994; McArthur *et al.*, 2001; Jenkyns *et al.*, 2002), but are in the range of the Burdigalian - Langhian (early to middle Miocene) marine water (0.7083 — 0.7088, Koepnick *et al.*, 1985; McArthur *et al.*, 2001) (Fig. 9). The increase in radiogenic strontium suggests that: i) Burdigalian - Langhian marine waters were involved in the dolomitization process; ii) the radiogenic Sr resulted from the leaching of detrital clays that interacted with the dolomitizing fluid, either in adjacent strata or in

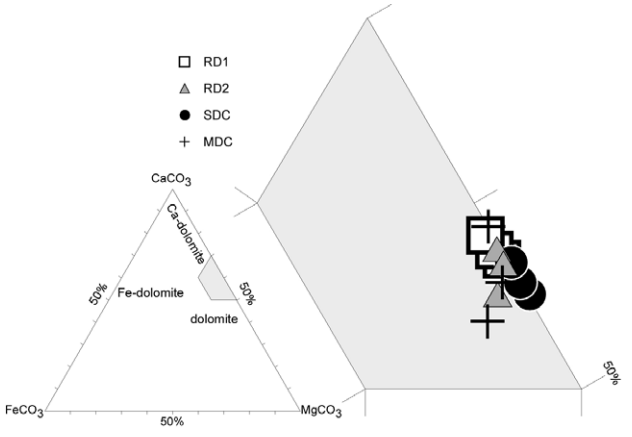

FIGURE 8 | Ternary diagram showing the elemental composition of dolomite types obtained by WDS (wavelength dispersion spectroscopy) electron microprobe. The data represents mean, minimum and maximum values for each dolomite type.

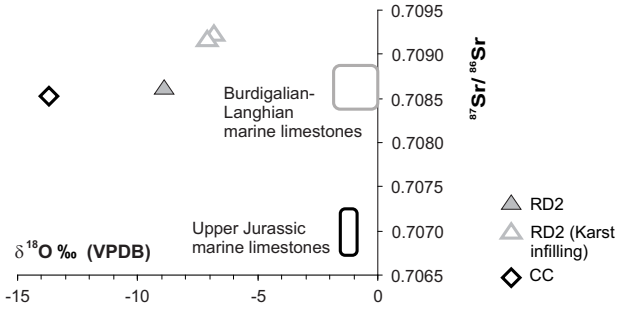

FIGURE 9 | Strontium isotope composition ($^{87}Sr/^{86}Sr$) of RD2 and CC. The oxygen isotope composition corresponds to the same sample analyzed for the $^{87}Sr/^{86}Sr$ ratio, except for calcite cement where mean value is used. Range of values for Upper Jurassic and Burdigalian - Langhian marine limestones are according to Koepnick *et al.* (1985); Jones *et al.* (1994); McArthur *et al.* (2001); and Jenkyns *et al.* (2002). Oxygen isotope composition of Upper Jurassic and Burdigalian - Langhian marine limestones is according to Allan and Wiggins (1993).

the karstic system; or iii) the dolomitizing fluid interacted with other siliciclastic sediments (Allan and Wiggins, 1993; Duggan *et al.*, 2001; Marfil *et al.*, 2005; Davies and Smith, 2006). The prevalent marine conditions existing during the Burdigalian and Langhian could allow the influx of downward marine waters through active extensional faults (option i). However, the occurrence of clay minerals in the karst infillings indicates that the source of this radiogenic strontium was, at least locally, the illitization of the clay coats (option ii). This process releases fluids enriched in Mg^{2+}, Fe^{2+}, Na^{+}, Ca^{2+} and Sr^{2+} that could be used in diagenetic reactions as dolomitization (Worden and Morad, 2003). However, the participation of fluids that interacted with radiogenic siliciclastic sediments has not been ruled out (option c). Taking into account a Formation. temperature around 60ºC, suggested from petrographic data, the $\delta^{18}O$ values of replacive dolomites replacive dolomite 1 and replacive dolomite 2 indicate precipitation from a fluid with an isotopic composition between -6 and -3‰ VSMOW. These values are compatible with precipitation from meteoric waters mixed with marine waters.

A local source of radiogenic strontium associated with the alteration of detrital clay minerals is also indicated by the higher $^{87}Sr/^{86}Sr$ ratios (ranging from 0.709137 to 0.709202) of the dolomitized infillings in RD2 compared to those of the host replacive dolomite 2 (0.708607; Fig. 9, Table 4). The illitization was wholly or partly simultaneous with the dolomitization event, enabling the local modification of the isotopic composition of the dolomitizing fluids that affected the carbonate infillings. The highly radiogenic values obtained in the accompanying clay minerals within the infillings (between 0.724652 and 732111; Table 2; 4) support the formulated hypothesis.

The oxygen isotope composition of the saddle dolomite cement (ranging from -8.9 to -6.8‰ VPDB) is also consistent with precipitation at high temperatures (Allan and Wiggins, 1993). Saddle dolomite is commonly reported to form at temperatures between 60 and 150ºC (Radke and Mathis, 1980). The similar $\delta^{18}O$ values, $\delta^{13}C$ values, cathodoluminescence patterns and the uniformity in minor and trace element composition of replacive dolomite 1, replacive dolomite 2 and saddle dolomite cement indicates that they formed from similar parent fluids, in a continuous event. The occurrence of dolomite-planar textures (replacive dolomite 1 and replacive dolomite 2) together with non planar textures (saddle dolomite cement) could indicate that the formation temperature does not exceed 60ºC (Gregg and Sibley, 1984; Sibley and Gregg, 1987). According to the $\delta^{18}O$ values of saddle dolomite cement, and using the dolomite-water fractionation equation (Friedman and O'Neil, 1977), the parent fluid would have had $\delta^{18}O$ between -4.4 and -2.3‰ VSMOW if precipitation temperature had been 65ºC, and less negative at higher temperature. These values are consistent with mixing of meteoric and marine waters.

The petrologic observations performed with ESEM and TEM point out that fibrous-type I/S probably resulted from a progressive recrystallization of detrital clays. I/S originates from the transformation of smectite-rich clays with burial and heating, having illite as an end product in mesodiagenesis at about 110ºC (Worden and Morad, 2003). Therefore, it could be accepted that this temperature was not exceeded during Formation. of replacive dolomite 1, replacive dolomite 2 and saddle dolomite cement.

The oxygen isotope composition of milky-white dolomite cement (from -11.9 to -11.4‰ VPDB) may indicate a higher temperature of Formation. than that of the previous dolomites (Allan and Wiggins, 1993). This higher temperature could result either from increasing burial conditions (3‰ equates to roughly 12ºC, and in a rift setting with possible elevated geothermal gradient that may only be around 200-300 meters) and from the input of hotter fluids. Hydrothermal fluids entered the basin during the Neogene postrift at late Miocene times (Varela *et al.*, 2005) when the maximum burial depth was reached (Clavell and Berastegui, 1991; Vallaure and Mallo-García, 2005). Milky-white dolomite cement partially obliterated the secondary porosity generated during the subaerial exposition and karstification stage (Fig. 10E-3).

The $\delta^{13}C$ values of all dolomites are within the range of Upper Jurassic marine limestones. It indicates that carbon isotope composition of all dolomites was little modified during burial, and fluids forming replacive and cement dolomites were buffered by the host limestones and/or earlier dolomites.

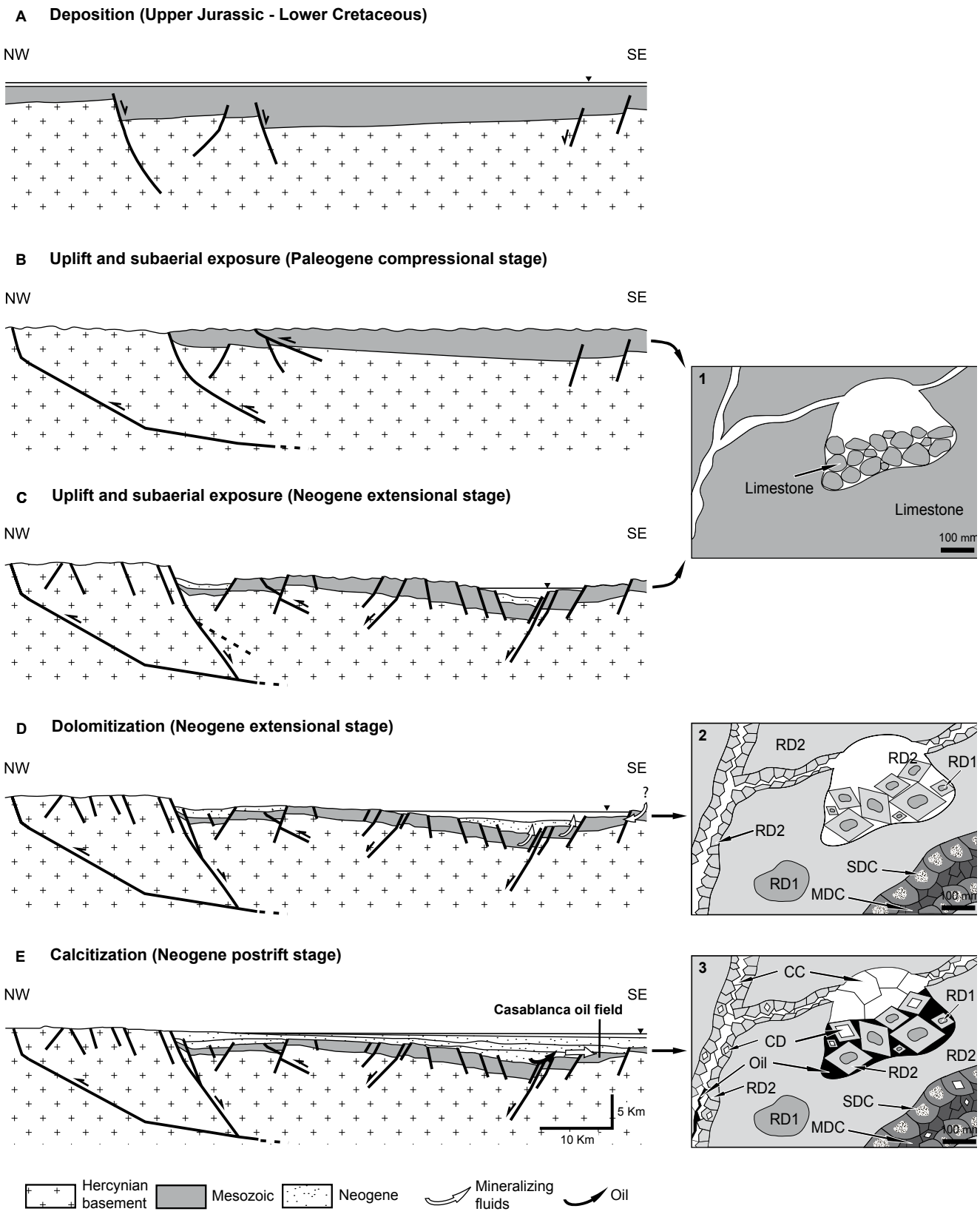

FIGURE 10 Proposed model of diagenetic evolution from sedimentation of the original limestone (Upper Jurassic - Lower Cretaceous) to oil emplacement (Pliocene) in the Casablanca oil field. RD1: Replacive Dolomite 1; RD2: Replacive Dolomite 2; SDC: Saddle Dolomite Cement; MDC: Milky-white Dolomite Cement; CC: Calcite Cement.

Calcite precipitation and oil emplacement

Calcite cement post-dates all dolomite types, and is associated to a partial but widespread calcitization of previous dolomites (Fig. 10). The oxygen isotope composition (between -14.3 and -13.1‰ VPDB) and the Mg/Ca, Sr/Ca and Ca/Fe molar ratios (mean value of 0.14, 0.013 and 276, respectively; Table 2) are characteristic of Formation. waters (McIntire, 1963; Moore and Druckman, 1981). Assuming a temperature interval from 60 to 110ºC, as there is no evidence of burial disruption between precipitation of saddle dolomite cement and calcite cement, and using the equation temperature of Craig (1965) for mean $\delta^{18}O$ composition of the calcite cement (-13.7‰ VPDB), it is estimated that this calcite cement precipitated from fluids with $\delta^{18}O$ values between -5.5 and +1.4‰ SMOW. This composition is within the range of meteoric water mixed with either Formation. waters or marine waters.

The strontium isotope composition of the calcite cement (0.708521) is within the range of the Burdigalian - Langhian marine water (0.7083 — 0.7088, Koepnick *et al.*, 1985; McArthur *et al.*, 2001), indicating that precipitation of this cement may have occurred from a Burdigalian - Langhian derived marine water trapped in Neogene sediments and expelled by compaction during burial. This marine water would have mixed with meteoric water to obtain their negative $\delta^{18}O$ values. Normal faults may have served as pathway for upward circulation of these mineralizing fluids to more permeable zones (Fig. 10E). This interpretation is coherent with later oil expulsion and vertical migration from the Burdigalian - Langhian source rock of the Casablanca oil field through normal faults (Matias *et al.*, 2010; Varela *et al.*, 2005).

Partial calcitization of dolomite took place in close association with precipitation of the calcite cement. Due to the association of this calcite with oil, the most probable origin of calcitization is associated with circulation of organic acid-enriched fluids expelled from the source rocks as a precursor to oil emplacement. These acid fluids would have dissolved the host dolomite and inherited the $^{87}Sr/^{86}Sr$ ratio. The resulting calcitized dolomite was enriched in Sr and depleted in Fe with respect to the precursor dolomite (Table 2). The minor and trace element compositions suggest calcitization from formation. fluids (*c.f.* Budai *et al.*, 1984) and, therefore, a common origin of calcitized dolomite with the calcite cement would be reasonable.

Although the calcitization process affected all dolomite types, it did not act on them equally. The stability and internal ordering of the dolomite crystals (stoichiometry) seems to be the cause of this selective and differential dolomite calcitization (Dorobek *et al.*, 1993; Nader *et al.*, 2003). Less stable, nonstoichiometric, poorly-ordered dolomite tends to be altered more readily than more stable, stoichiometric, better-ordered dolomite. Petrological observations show that milky-white dolomite cement is deeply calcitized, which probably is associated with the highest stoichiometrical variability compared to the other dolomite types (Fig. 8; Table 2). This is also the case for replacive dolomite 2, where calcitization mainly affected the less stoichiometric centers of the remaining replacive dolomite 1.

Petrographic data indicate that pyrite precipitated after the late calcite and calcitization of dolomite. The precipitation of some rare or "exotic" minerals in carbonate reservoirs, such as pyrite, barite, kaolinite, as well as dickite, quartz, gypsum, and fluorite, is thought to occur prior or during the hydrocarbon arrival (Davies and Smith, 2006; Neilson and Oxtoby, 2008). At the Casablanca-1A core well samples nothing but pyrite was identified as exotic cement, and in a very scarce content. Fe presumably came from the dissolved dolomite.

The corrosion affecting calcite and dolomite is probably associated to a late stage of hydrocarbon emplacement as previously reported in the Valencia Trough oil fields (Clavell and Berastegui, 1991; Klimowitz *et al.*, 2005; Varela *et al.*, 2005; Matias *et al.*, 2010). According to the later authors, the oil migration occurred at late Miocene- early Pliocene times. This corrosion enhanced vug and fracture porosity increasing reservoir quality. It is thought that many wells would be unproductive without this diagenetic stage. In the studied well of the Casablanca field, oil circulated mainly through intercrystalline porosity and through enhanced fracture and vug porosity (Fig. 10E-3).

Similar diagenetic sequences such as the one proposed in this study have been presented for other oil fields situated in the Valencia Trough, such as the Amposta oil field (Playà *et al.*, 2010).

CONCLUSIONS

The study of the Upper Jurassic carbonate core samples from the Casablanca-1A well (Casablanca Oil Field, offshore Spain) reveals three main diagenetic stages: i) a pre-dolomitization stage which involves uplift and subaerial exposure; ii) a dolomitization stage which results in the complete replacement of the host rock; and iii) a post-dolomitization stage characterized by calcite cementation and the emplacement of oil.

The Mesozoic limestone succession was uplifted and subaerially exposed between the Paleogene compression and the Neogene extension resulting in the karstification of

the host rock. This process created significant vug porosity, and enhanced fracture porosity as well, that was partially filled by carbonate sediments and clays derived from the weathering of the host limestone and other lithologies cropping out in the area.

Following the Neogene extension, the host rock and the karst infillings were dolomitized during progressive burial. Petrographic and geochemical data indicate that the replacive dolomite 1 (replacive dolomite 1), replacive dolomite 2 (replacive dolomite 2) and saddle dolomite cement are partially cogenetic and formed from similar parent fluids in a continuous process. replacive dolomite 1, replacive dolomite 2 and saddle dolomite cement precipitated at increasing temperature (between 60º and 110ºC), most likely from a mix of meteoric and marine water. Illitization of the clay coats would have been locally responsible for the high-radiogenic signature of dolomites. Milky dolomite cement precipitated with increasing burial conditions and/or by the arrival of hydrothermal fluids during the late Miocene.

Subsequent to milky-white dolomite cement Fm. and prior to (or during) the oil emplacement in the Pliocene, calcite cementation and associated calcitization of dolomite took place. This process is most probably associated with circulation of organic acid-enriched Burdigalian Langhian marine water trapped in the sediments and expelled by compaction during burial. This marine water would have mixed with meteoric water to obtain their negative $\delta^{18}O$ values. Normal faults were the conduits for upward migration of organic acid-enriched fluids and hydrocarbons, which were expelled from Burdigalian - Langhian source rocks.

The reported diagenetic sequence reflects the obliteration of porosity by successive cement precipitations in a dense dolomitic body. Results indicate that the reservoir quality of the studied core samples is related to the intercrystalline, fracture and vug porosity remaining after late calcite cementation. This porosity was enhanced by the corrosion associated with the acid source-rock derived fluids during oil migration.

ACKNOWLEDGMENTS

The authors gratefully acknowledge Mateu Esteban (Carbonates International Iberia S.L., Mallorca-Spain), María Ochoa (Repsol), Albert Permanyer (Universitat de Barcelona) and Montserrat Inglés (Universitat de Barcelona) for their remarks, suggestions and scientific contributions. Repsol is thanked for sample availability. We thank Jim Hendry and Ana Alonso-Zarza for their constructive comments on an earlier version of the manuscript. We are grateful to Xavier Llovet, Xavier Alcobé, Javier García Veigas, Joaquim Portillo and Joaquim Perona from the "Serveis Cientifics i tecnològics" of the Universitat de Barcelona for technical assistance; and to José Manuel Fuenlabrada from the "CAI de geocronología y geoquímica isotópica" of the Universidad Complutense de Madrid for strontium isotope analyses. This research was supported by the Spanish Government Project CGL2010-18260 and the "Grup Consolidat de Recerca Geologia Sedimentària" 2009SGR-1451.

REFERENCES

Allan, J.R., Wiggins, W.D., 1993. Dolomite Reservoirs. Geochemical Techniques for Evaluating Origin and Distribution. American Association of Petroleum Geologists, Tulsa, Continuing Education Course Note Series, 36, 129pp.

Baqués, V., Travé, A., Labaume, P., Benedicto, A., Soliva, R., 2011. Differences between Neogene pre-rift and syn-rift karsts from petrological and geochemical analysis of their infillings. In: Ruiz-Sánchez, F.J., Santiesteban, C. (eds.) Documentos sobre el Terciario de Iberia a inicios del Siglo XXI. Valencia, 9-12.

Baqués, V., Travé, A., Roca, E., Marin, M., Cantarero, I., 2012. Geofluids behaviour in successive extensional and compressional events: a case study from the south-western end of the Vallès-Penedès fault (Catalan Coastal Ranges, NE Spain). Petroleum Geoscience, 18, 17-31.

Budai, J.M., Lohmann, K.C., Owen, R.M., 1984. Burial dedolomite in the Mississippian Madison Limestone, Wyoming and Utah thrust belt. Journal of Sedimentary Petrology, 54(1), 276-288.

Cabrera, Ll., Roca, E., Garcés, M., de Porta, J., 2004. Estratigrafía y evolución tectonosedimentaria oligocena superior-neógena del sector central del margen catalán (Cadena Costero-Catalana). In: Vera, J.A. (ed.). Geología de España. Sociedad Geológica de España, Madrid, Instituto Geológico y Minero de España, 569-572.

Clauer, N., Chaudhuri, S., 1995. Clays in Crustal Environments: Isotope Dating and Tracing. Springer-Verlag. 369pp.

Clauer, N., Liewig, N., Ledesert, B., Zwingmann, H., 2008. Thermal history of Triassic sandstones from the Vosges Mountains-Rhine Graben rifting area, NE France, based on K-Ar illite dating. Clay Minerals, 43, 363-379.

Clavell, E., Berastegui, X., 1991. Petroleum geology of the Gulf of Valencia. In: Spencer, A.M. (ed.). Generation, accumulation and production of Europe's hydrocarbons. Oxford, Special publication of the European Association of Petroleum Geologists, 1, 355-368.

Craig, H., 1965. The measurement of oxygen isotope palaeotemperatures. In: Tongiorgi, E. (ed.). Stable isotopes in oceanographic studies and palaeotemperatures. Pisa, Consiglio Nazionale delle Ricerche Laboratorio di Geologia Nucleare, 166–182.

Davies, G.R., Smith, L.B., 2006. Structurally controlled hydrothermal dolomite reservoir facies: an overview. American Association of Petroleum Geologists Bulletin, 90, 1641-1690.

Demaison, G., Bourgeois, F.T., 1984. Environment of deposition of Middle Miocene (Alcanar) Carbonate Source Beds, Casablanca Field, Tarragona Basin, Offshore Spain. In: Palacas, J.G. (ed.). Petroleum Geochemistry and source rock potential of carbonate rocks, American Association of Petroleum Geologists Studies in Geology, 18, 151-161.

Dorobek, S.L., Smith, T.M., Whitsitt, P.M., 1993. Microfabrics and geochemistry of meteorically altered dolomite in Devonian and Mississippian carbonates, Montana and Idaho. In: Rezak, R., Lavoie, D.L. (eds.). Carbonate Microfabrics. Frontiers in Sedimentary Geology, 205-235.

Dromgoole, E.L., Walter, L.M., 1990. Iron and manganese incorporation into calcite: Effects of growth kinetics, temperature and solution chemistry. Chemical Geology, 81, 311-336.

Duggan, J.P., Mountjoy, E.W., Stasiuk, L.D., 2001. Fault-controlled dolomitization at Swan Hills Simonette oil field (Devonian), deep basin west-central Alberta, Canada. Sedimentology, 48, 301-323.

Esteban, M., 1973. Petrología de las calizas Cretácicas del Sector Central de los Catalánides (Prov. de Tarragona y Barcelona). Doctoral Thesis. Barcelona, Universitat de Barcelona, unpublished, 425pp.

Esteban, M., 1991. Palaeokarst: case histories. In: Wright, V.P., Esteban, M., Smart, P.L. (eds.). Palaeokarsts and Palaeokarstic Reservoirs. Postgraduate Research Institute for Sedimentology, University of Reading, 120-46.

Esteban, M., 1998. El complejo Basal Mioceno del Mediterráneo. Internal report, REPSOL, unpublished.

Friedman, I., O'Neil, J.R., 1977. Compilation of stable isotope fractionation factors of geochemical interest. In: Fleischer, M: (ed.). Data of Geochemistry. Reston, VA, U.S. Geological Survey Professional Paper 440-KK, 6th Ed..

Gaspar-Escribano, J.M., García-Castellanos, D., Roca, E., Cloetingh, S., 2004. Cenozoic verical motions of the Catalan Coastal Ranges (NE Spain): The role of tectonics, isostasy, and surface transport. Tectonics, 23, TC1004, DOI:10.1029/2003TC001511

Gregg, J.M., Sibley, D.F, 1984. Epigenetic dolomitization and the origin of the xenotopic dolomite texture. Journal of Sedimentary Petrology, 54, 908-931.

Gregg, J.M., 2004. Basin fluid flow, base-metal sulphide mineralization and the development of dolomite petroleum reservoirs. In Braithwaite, C.J.R., Rizzi, G., Darke, G. (eds.). The geometry and petrogenesis of dolomite hydrocarbon reservoirs. London, Geological Society (Special Publications), 157 - 175.

Jenkyns, H.C., Jones, C.E., Gröcke, D.R., Hesselbo, S.P., Parkinson, D.N., 2002. Chemostratigraphy of the Jurassic System: applications, limitations and implications for palaeoceanography. Journal of the Geological Society of London, 159, 351-378.

Jones, C.E., Jenkyns, H.C., Coe, A.L., Hesselbo, S.P., 1994. Strontium isotope variations in Jurassic and Cretaceous seawater. Geochimica et Cosmochimica Acta, 58, 3061-3074.

Katz, A., 1973. The interaction of magnesium with calcite during crystal growth at 25-90ºC and one atmosphere. Geochimica et Cosmochimica Acta, 37, 1563-1586.

Katz, A., Sass, E., Starinsky, A., Holland, H.D., 1972. Strontium behaviour in the aragonite-calcite transformation: An experimental study at 40-98ºC. Geochimica et Cosmochimica Acta, 36, 481-496.

Klimowitz, J., Hernández, E., Serrano, A., 2005. A field trip guide book. The Mediterranean Basin (Catalan costal range onshore analogues). In: Martínez del Olmo (ed.). Asociación de Geólogos y Geofísicos Españoles del Petróleo (AGGEP)-XXV Aniversario, 187-208.

Koepnick, R.B., Burke, W.H., Denison, R.E., Hetherington, E.A., Nelson, H.F., Otto, J.B., Waite, L.E., 1985. Construction of the seawater $^{87}Sr/^{86}Sr$ curve for the Cenozoic and Cretaceous: supporting data. Chemical Geology, 58, 55-81.

Land, L.S., 1980. The isotopic and trace element geochemistry of dolomite: the state of art. In: Zenger, D.H., Dunham, J.B., Ethington, R.L. (eds.). Concepts and models of dolomitization. Society of Economic Paleontologists and Mineralogists, 28 (Special Publications), 87-110.

Lomando, A.J., Harris, P.M., Orlopp, D.E., 1993. Casablanca Field, Tarragona Basin, Offshore Spain: A karsted carbonate reservoir. In: Fritz, R.D., Wilson, J.L., Yurewicz, D.A. (eds.). Paleokarst related hydrocarbon reservoirs, Society of Economic Paleontologists and Mineralogists, Core Workshop, 18, 201-225.

Lonnee, J., Machel, H.G., 2006. Pervasive dolomitization with subsequent hydrothermal alteration in the Clarke Lake gas field, Middle Devonian Slave Point Formation, British Columbia, Canada. American Association Petroleum Geologists Bulletin, 90, 1739-1761.

Machel, H.G., 1997. Recrystallization versus neomorphism, and the concept of significant recrystallization in dolomite research. Sedimentary Geology, 131, 161-168.

Machel, H.G., 2004. Concepts and models of dolomitization: a critical reappraisal. In: Braithwaite, C.J.R., Rizzl, G., Darke, G. (eds). The geometry and petrogenesis of dolomite hydrocarbon reservoirs. London, Geological Society, 235 (Special Publications), 7-63.

Marfil, R., Caja, M.A., Tsige, M., Al-Aasm, I.S., Martín-Crespo, T., Salas, R., 2005. Carbonate-cemented stylolites and fractures in the Upper Jurassic limestones of the eastern Iberian Range, Spain: A record of palaeofluids composition and thermal history. Sedimentary Geology, 178, 237-257.

Martín-Martín, J.D., Travé, A., Gomez-Rivas, E., Sizun, J.P., Salas, R., Gómez-Gras. D., Vergés, J., 2010. Fault–associated dolomites in the Benicàssim area, Maestrat Basin, E. Spain – Macro– to micro–scale fluid flow in carbonates. Society of Petroleum Engineers, 72nd European Association of Geoscientists and Engineers Conference and Exhibition 2010, Incorporating SPE EUROPEC 2010 4, 2980-2984.

Matias, H.C, Vila Pont, J., Martin Banon, J.J., Arnez Espinosa, L.R., Loza Peirano, J., Bertoni, C., 2010. Exploration challenges in the Valencia Trough, offshore Spain – The Lubina and Montanazo discoveries. Society of Petroleum Engineers, 72nd European Association of Geoscientists and Engineers Conference and Exhibition 2010, Incorporating SPE EUROPEC 2010 4, 2980-2984.

McArthur, J.M., Howarth, R.J., Bailey, T.R., 2001. Strontium Isotope Stratigraphy: LOWESS Version 3: Best Fit to the Marine Sr-Isotope Curve for 0-509 Ma and Accompanying Look-up Table for Deriving Numerical Age. The Journal of Geology, 109, 155-170.

McIntire, J.W., 1963. Trace element partition coefficients – a review of theory and applications to geology. Geochimica et Cosmochimica Acta, 27, 1209-1264.

Moore, C.H., Druckman, Y., 1981. Burial diagenesis and porosity evolution, Upper Jurassic Smackover, Arkansas and Louisiana. American Association of Petroleum Geologists Bulletin, 65, 597-628.

Moraes, M.A.S., De Ros, L.F., 1990. Infiltratred clays in fluvial Jurassic sandstones of Recôncavo Basin, northeastern Brazil. Journal of Sedimentary Geology, 60, 089-819.

Nadal, J., 2001. Estudi de la dolomitització del Juràssic Superior-Cretaci Inferior de la Cadena Ibèrica Oriental i la Cadena Costanera Catalana: Relació amb la segona etapa de rift mesozoica. Doctoral Thesis. Barcelona, Universitat de Barcelona, unpublished, 416pp.

Nader, F.H., Swennen, R., Ottenburgs, R., 2003. Karst-meteoric dedolomitization in Jurassic carbonates, Lebanon. Geologica Belgica, 64 (1,2), 3-23.

Neilson, J.E., Oxtoby, N.H., 2008. The relationship between petroleum, exotic cements and reservoir quality in carbonates – A review. Marine and Petroleum Geology, 25, 778-790.

Nielsen, P., Swennen, R., Keppens, E., 1994. Multiple-step recrystallization within massive ancient dolomite units: an example from the Dinantian of Belgium. Sedimentology, 41, 567-584.

Orlopp, D.E., 1988. Casablanca Oilfied, Spain: a karsted carbonate trap at the shelf edge. Proceedings of the Offshore Technology Conference, OTC 5734, 441-448.

Permanyer, A., Salas, R., 2005. Integrated thermal model, diagenetic history and oil correlation in western Mediterranean, Spain. IV ALAGO Workshop on Basin Modelling, Buenos Aires, Communication.

Playà, E., Travé, A., Caja, M.A., Salas, R., 2010. Diagenesis of the Amposta offshore oil reservoir (Amposta Marino C2 well, Lower Cretaceous, Valencia Trough, Spain). Geofluids, 10, 314-333.

Radke, B.M., Mathis, R.L., 1980. On the formation. and occurrence of saddle dolomite. Journal of Sedimentary Petrology, 50, 1149-1168.

Rameil, N., 2008. Early diagenetic dolomitization and dedolomitization of Late Jurassic and earliest Cretaceous platform carbonates: A case study from the Jura Mountains (NW Switzerland, E France). Sedimentary Geology, 212, 70-85.

Roca, E., 1994. La evolución geodinámica de la Cuenca Catalano-Balear y áreas adyacentes desde el Mesozoico hasta la actualidad. Acta Geológica Hispánica, 29 (1), 3-25.

Rossi, C., Goldstein, R.H., Marfil, R., Salas, R., Benito, M.I., Permanyer, A., de la Peña, J.A., Caja, M.A., 2001. Diagenetic and oil migration of the Kimmeridgian Ascla Formation, Maestrat Basin, Spain. Marine and Petroleum Geology, 18, 287-306.

Salas, 1987. El Malm i el Cretaci inferiorentre el Massís del Garraf i la Serra d'Espadà. Anàlisi de conca. Doctoral Thesis, Barcelona, Universitat de Barcelona, unpublished, 345pp.

Salas, R., Guimerà, J., Mas, R., Martín-Closas, C., Meléndez, A., Alonso, A., 2001. Evolution of the Mesozoic central Iberian Rift System and its Cainozoic inversion (Iberian chain). In: Zeigler, P.A., Cavazza, W., Robertson, A.H.F., Crasquin-Soleau, S. (eds.). Peri-Tethys Memoir 6: Pery-Tethyan Rift/Wrench Basin and Passive Margins. Paris, Memoirs du Museum National d'Histoire Naturelle (France), 186, 145-185.

Sant'Anna, L.G., Clauer, N., Cordani, U.G., Ricconimi, C., Velázquez, V.F., Liewig, N., 2006. Origin and migration timing of hydrothermal fluids in sedimentary rocks of the Paraná Basin, South America. Chemical Geology, 230, 1-21.

Seemann, U., Pümpin, V.F., Casson, V.F., 1990. Amposta oil field. In: American Association of Petroleum Geologists treatise of Petroleum Geology. Atlas of oil and gas fields, A-017, 1-20.

Sibley, D.F., Gregg, J.M., 1987. Classification of dolomite rock textures. Journal of Sedimentary Petrology, 57, 967-975.

Stoessell, R.K., Klimentidis, R.E., Prezbindowski, D.R., 1987. Dedolomitization in Na-Ca-Cl brines from 100° to 200°C at 300 bars. Geochimica et Cosmochimica Acta, 51, 847-855.

Torres, J., Bois, C., Burrus, J., 1993. Initiation and evolution of the Valencia Trough (western Mediterranean): constraints from deep seismic profiling and subsidence analysis. Tectonophysics, 228, 57-80.

Travé, A., Calvet, F., 2001. Syn-rift geofluids in fractures related to the early-middle Miocene evolution of the Vallès-Penedès half-graben (NE Spain). Tectonophysics, 336, 101-120.

Travé, A., Calvet, F., Soler, A., Labaume, P., 1998. Fracturing and fluid migration during Palaeogene compression and Neogene extension in the Catalan Coastal Ranges, Spain. Sedimentology, 45, 1063-1082.

Vallaure, T., Mallo-García, J., 2005. Metodología para un estudio de la viabilidad de inyección y almacenamiento de CO_2 en el Campo Casablanca, Mediterráneo, España. In: Martínez del Olmo (ed.). Asociación de Geólogos y Geofísicos Españoles del Petróleo (AGGEP)-XXV Aniversario, 169-177.

Varela, J., Vicente-Bravo, J.C., Navarro, J., Esteban, M., Martinez del Olmo, W., 2005. The Oil Fields in the Spanish Mediterranean Sea. In: Martínez del Olmo (ed.). Asociación de Geólogos y Geofísicos Españoles del Petróleo (AGGEP)-XXV Aniversario, 121-129.

Warren, J., 2000. Dolomite: occurrence, evolution and economically important associations. Earth Science Review, 52, 1-81.

Watson, H.J., 1982. Casablanca Field, offshore Spain, a paleogeomorphic trap. In: Halbouty, M.T. (ed.). The deliberate search for the subtle trap. Tulsa, American Association of Petroleum Geologists, Memoir 32, 237-250.

Worden, R.H., Morad, S., 2003. Clay minerals in sandstones: controls on formation, distribution and evolution. In: Worden, R.H., Morad, S. (eds.). Clay mineral cements in sandstones. Special Publication of the International Association of Sedimentologists, 34, Blackwell Publishing, 3-41.

Manuscript received January 2010;
revision accepted July 2011;
published Online October 2012.